# Magnetic excitations in terbium antimonide

T. M. Holden, E. C. Svensson, and W. J. L. Buyers
*Atomic Energy of Canada Limited, Chalk River, Ontario, Canada K0J 1J0*

O. Vogt
*Laboratorium für Festkorperphysik, Eidgenössische Technische Hochschule, Zürich, Switzerland*
(Received 27 June 1974)

The magnetic-excitation spectrum of the singlet-ground-state antiferromagnet TbSb has been studied by neutron inelastic scattering. At 4.4 K, the dispersion relations for the two lowest branches of the spectrum were determined, and evidence was also obtained for transitions between the ground state and the seventh and ninth excited states of the $Tb^{3+}$ ion. Measurements were also carried out at several other temperatures both below and above $T_N$ ($14.9 \pm 0.2$ K). At 4.4 K, the lowest branch has a large energy gap (frequency $0.54 \pm 0.04$ THz) caused by crystalline-field effects. The gap decreases as the temperature is raised and near $T_N$ the spin-wave scattering merges with a broad distribution of quasielastic critical scattering whose intensity reaches a maximum at $T_N$. Above $T_N$, the critical scattering gradually decreases with increasing temperature. The quasielastic scattering at the zone boundary has a somewhat larger frequency width than that at the zone center and also exhibits a weak shoulder in the temperature range 20–40 K. This behavior is inconsistent with current theories based on truncated-energy-level schemes, which predict that there should be a well-defined mode in the disordered phase whose frequency tends to the crystal-field splitting $\Delta$ at high temperature and to zero as $T \rightarrow T_N$. Exchange and crystal-field parameters for TbSb have been obtained by analyzing the results at 4.4 K in terms of a pseudoboson theory which takes into account transitions between the ground state and all 12 excited states of the lowest spin-orbit multiplet of the $Tb^{3+}$ ion ($J = 6$). A very good description of the observed frequencies and intensities is obtained.

## I. INTRODUCTION

Terbium antimonide is an intermetallic rare-earth compound which exhibits[1] antiferromagnetic order below about 15 K. This compound is particularly interesting because the ground state of the $Tb^{3+}$ ion in a ıbic crystalline field is a singlet and has zero moment in the absence of exchange interactions. Exchange interactions, however, induce a moment in the ground state by admixture of excited-state wave functions into the ground-state wave function. A critical ratio of exchange to crystal field has to be exceeded to ensure a net magnetic moment, and this criterion is met in TbSb.

Singlet-ground-state systems were first discussed over 30 years ago by Van Vleck.[2] Trammell[3] gave a clear formulation of the problem and used the crystalline-field model to explain the directions of easy magnetization exhibited by several rare-earth phosphides. More recently Cooper,[4] Wang and Cooper,[5] Pink,[6] and Hsieh and Blume[7] have calculated the magnetic-excitation spectra of these materials, usually within the framework of a truncated-energy-level scheme for the magnetic ion, and Cooper[8] and Birgeneau[9] have reviewed these contributions. These simplified energy-level schemes have taken the form of either a singlet ground state with a singlet excited state or a singlet ground state with a triplet excited state, and, by use of the random-phase approximation, the magnetic-excitation spectrum and its temperature dependence have been obtained. These theories predict that above the ordering temperature the long-wavelength transverse exciton modes have finite frequency, but that they go to zero at the ordering temperature. Only very recently have experimental results become available to test these theoretical predictions in detail, and there are still many interesting questions to be answered by experimental studies of the spectra of magnetic excitons in singlet-ground-state systems. For example, the adequacy of simplified models of the energy-level scheme can be tested as can also the prediction of a soft mode at the transition temperature.

The present neutron inelastic scattering measurements of magnetic excitations in a single crystal of TbSb demonstrate the inadequacy not only of simplified models such as the singlet-triplet model but also of the concept of a soft mode in the nonordered phase. A theory has been developed which gives good agreement with the low-temperature data provided all levels of the ground multiplet are included. A preliminary account of this work has already been published.[10]

Many measurements[11] of the susceptibility and specific heat of singlet-ground-state systems have been reported, and, until recently, these were the only types of measurement available for investigating the behavior of singlet ground states. Of

particular relevance are the measurements of the susceptibility of TbSb-based solid solutions by Cooper and Vogt.[12] With the application of neutron scattering as a spectroscopic tool for studying crystal-field excitations much more detailed information has become available. Neutron inelastic scattering studies on CeAs and CeSb,[13] TmSb,[14] hcp Pr,[15] fcc Pr and $Pr_3Tl$[16] and many other Pr compounds[17] have now been published covering a wide range of behavior. For TmSb the exchange interactions are negligible, for single crystals of hcp Pr the exchange just fails to induce magnetic order, and for fcc Pr and $Pr_3Tl$ the exchange is just sufficient to induce weak magnetic ordering. These cases contrast with TbSb, for which the exchange is some three times larger than that required (see, for instance, Cooper[4]) to induce magnetic order, yet crystal-field effects still dominate the spectrum. For Tb metal,[18] as an extreme case, exchange interactions are much larger than crystal-field effects and the latter only contribute to the magnetic anisotropy.

TbSb crystallizes in the rocksalt structure and below $14.9 \pm 0.2$ K[19] it is a type-II antiferromagnet with alternating antiparallel (111) sheets of spins[1] and with spin direction along the [111] axis. The magnetic moment per Tb ion in the ordered phase was determined[1] from the intensity of the superlattice reflections to be $8.2\mu_B$. With a $g$ factor of 1.5, this corresponds to an average value of the total spin plus orbital angular momentum (referred to hereafter as spin) $\langle S_z \rangle = 5.45$. This is only slightly less than the free-ion value of 6, demonstrating the extent of the mixing of the wave functions. Levy[20] has shown that there is a small rhombohedral distortion of the cubic cell below $T_N$. The deviation of the rhombohedral angle of the primitive unit cell from the value for a cubic cell is $0.15^\circ$ at 4.0 K and it falls smoothly to zero at $T_N$.

Cooper and Vogt[12] measured the paramagnetic susceptibility of solid solutions of $Tb_xY_{1-x}Sb$ and from the susceptibility of those alloys which did not order they deduced a crystal-field parameter and an exchange field relevant to TbSb. Their parameters proved to be a useful starting point in our analysis.

It is useful to review briefly the single-ion energy-level scheme of $Tb^{3+}$ in an effective magnetic field directed along the [111] direction since this gives immediate insight into the character of the magnetic excitations presented in Sec. II. The $^7F_6$ ground-state multiplet is split by the cubic crystal field into six levels which, in order of increasing energy, are designated as $\Gamma_1$, $\Gamma_4$, $\Gamma_5^{(2)}$, $\Gamma_2$, $\Gamma_5^{(1)}$, $\Gamma_3$. The energy-level scheme is shown in Fig. 1 and wave functions and energies calculated from a set of crystal-field parameters deduced from the present analysis (model A) in zero molecular field are given in Table I. The square of the average values[21] of $\langle S_z \rangle$ and the transition matrix elements for zero molecular field are given in Table II. In zero molecular field at 0 K, when only the ground state is populated, only the $\Gamma_1 \rightarrow \Gamma_4$ transition will be observed, but as the temperature is raised and various excited states become populated, other transitions will become visible. It is clear from Fig. 1 that the whole range of energies involved is easily accessible in neutron scattering experiments. A magnetic field, whether an applied field or a molecular field, mixes the crystal-field-only wave functions and removes the level degeneracies as shown in Fig. 1. Because of the mixing of wave functions the spin in the ground state is no longer zero but tends towards the full value of 6 as the magnitude of the molecular field increases. It is now possible to induce transitions from the mixed ground state to any of the higher excited states although certain transition matrix elements may be very small. The dashed line in Fig. 1 corresponds to the exchange field for TbSb given by model A and the corresponding energies, wave functions, and matrix elements are given in Tables III and IV. The effect of a rhombohedral distortion of the crystal field is to shift all the levels and to split a triplet state at zero molecular field into a doublet

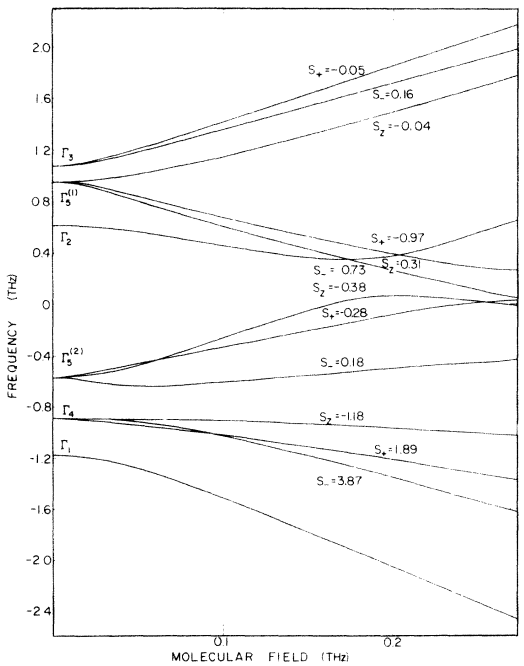


FIG. 1. Energy levels belonging to the $^7F_6$ multiplet of the $Tb^{3+}$ ion in the cubic crystal field of TbSb. The vertical dashed line corresponds to the exchange field for model A.

TABLE I. Energies and wave functions $|n\rangle$ in terms of the states $|S_z\rangle$ for $Tb^{3+}$ ions (total angular momentum $S=6$) in zero molecular field. $B_4^0=1.55\times10^{-4}$ THz and $B_6^0=B_2^0=0$.

| Energy of level, $E_n$ (THz) | Transition frequency, $\nu_n$ (THz) | | | | | | |
|---|---|---|---|---|---|---|---|
| | | $a$ | $\|6\rangle$ | $\|3\rangle$ | $\|0\rangle$ | $\|-3\rangle$ | |
| | | $b$ | $\|5\rangle$ | $\|2\rangle$ | $\|-1\rangle$ | $\|-4\rangle$ | |
| | | $c$ | $\|4\rangle$ | $\|1\rangle$ | $\|-2\rangle$ | $\|-5\rangle$ | $\|-6\rangle$ |
| −1.172 | 0 | $a$ | 0.398 | −0.380 | 0.629 | 0.380 | 0.398 |
| −0.893 | 0.279 | $b$ | 0.261 | −0.430 | 0.770 | 0.393 | |
| −0.893 | 0.279 | $c$ | −0.393 | 0.770 | 0.430 | 0.261 | |
| −0.893 | 0.279 | $a$ | 0.638 | −0.304 | 0.000 | −0.304 | −0.638 |
| −0.577 | 0.595 | $b$ | 0.540 | −0.676 | −0.421 | −0.273 | |
| −0.577 | 0.595 | $c$ | −0.273 | 0.421 | −0.676 | −0.540 | |
| −0.577 | 0.595 | $a$ | 0.540 | 0.034 | −0.643 | −0.034 | 0.540 |
| 0.614 | 1.786 | $a$ | −0.304 | −0.638 | 0.000 | −0.638 | 0.304 |
| 0.949 | 2.121 | $b$ | −0.607 | −0.416 | 0.286 | −0.613 | |
| 0.949 | 2.121 | $c$ | −0.613 | −0.286 | −0.416 | 0.607 | |
| 0.949 | 2.121 | $a$ | 0.223 | 0.596 | 0.437 | −0.596 | 0.223 |
| 1.060 | 2.232 | $b$ | 0.521 | 0.430 | 0.385 | −0.629 | |
| 1.060 | 2.232 | $c$ | 0.629 | 0.385 | −0.430 | 0.521 | |

and a singlet. The molecular field still gives much the same qualitative effect as when the rhombohedral distortion is absent although the exact details are different. In the paramagnetic phase there is no net distortion.

The general features of the excitation spectrum in the antiferromagnetic phase may be inferred from Fig. 1. We would expect to see transitions between the ground state and the first two or possibly three excited states in the frequency range 0.5–1.0 THz, and possibly transitions to the seventh and ninth states at ≈ 2.5 THz. In the paramagnetic regime we would expect to see features related to the allowed transitions between states in the limit of zero molecular field (in particular $\Gamma_1 \rightarrow \Gamma_4$ and $\Gamma_4 \rightarrow \Gamma_5^{(2)}$).

The theoretical interpretation of the low-temperature spectra is based upon an extension of Grover's[22] pseudoboson technique. This includes the mixing of the levels by the molecular field and by the interion exchange which gives rise to the wave-vector dependence of the excitation energies. The theory includes transitions between the ground state and all excited states of the lowest multiplet at $T=0$. The exchange and crystal-field parameters have been obtained by comparing the observed wave-vector dependence of the spin-wave energies with the results of this theory.

The detailed experimental results are described in Sec. II. The spin-wave theory is presented in Sec. III and the analysis and discussion in Secs. IV and V.

## II. EXPERIMENT

### A. Reciprocal lattice and antiferromagnetic domain structure

The Tb moments in the antiferromagnetic phase are constrained by the crystalline-field anisotropy to point along ⟨111⟩ directions. There are thus eight, presumably equally populated, antiferromagnetic domains in TbSb, but we need only consider the four domains with different spin directions, say along [111], $[\bar{1}\bar{1}1]$, $[\bar{1}11]$, and $[1\bar{1}1]$. The magnetic Brillouin zones are oriented differently for each of these four domains and their intersections with the $(1\bar{1}0)$ plane of the reciprocal lattice are shown in Fig. 2. Note that the $[\bar{1}11]$ and $[1\bar{1}1]$ domains give identical intersections with this plane. Note also that magnetic Bragg reflections of the form $n(\frac{1}{2}\frac{1}{2}\frac{1}{2})$ with $n$ odd are not observable by neutron scattering because the scattering vector is parallel to the spin direction.

For any wave-vector transfer $\vec{Q}$ there are in principle four different magnon wave vectors, one for each of the four domains. These may be converted to equivalent magnon wave vectors for the [111] domain as described fully in Sec. III. For example, for $\vec{Q}=2\pi a^{-1}(\frac{1}{2},\frac{1}{2},\frac{1}{2})$ the four reduced magnon wave vectors (units $2\pi a^{-1}$) are (0, 0, 0), $(\frac{1}{2},\frac{1}{2},-\frac{1}{2})$, $(\frac{1}{2},\frac{1}{2},-\frac{1}{2})$, and $(\frac{1}{2},\frac{1}{2},-\frac{1}{2})$. For $\vec{Q}=2\pi a^{-1}\times(0,0,1)$ the four reduced magnon wave vectors are identical and equal to $(-\frac{1}{2},-\frac{1}{2},\frac{1}{2})$. In general there are three distinct magnon wave vectors for

TABLE II. Values (Ref. 21) of $|\langle\Gamma_i|S_z|\Gamma_j\rangle|^2$ for zero molecular field.

| | $\Gamma_1$ | $\Gamma_4$ | $\Gamma_5^{(2)}$ | $\Gamma_2$ | $\Gamma_5^{(1)}$ | $\Gamma_3$ |
|---|---|---|---|---|---|---|
| $\Gamma_1$ | 0 | 14.000 | 0 | 0 | 0 | 0 |
| $\Gamma_4$ | 14.000 | 0.500 | 24.922 | 0 | 0.578 | 2.000 |
| $\Gamma_5^{(2)}$ | 0 | 24.922 | 7.188 | 4.417 | 5.291 | 0.182 |
| $\Gamma_2$ | 0 | 0 | 4.417 | 0 | 9.583 | 0 |
| $\Gamma_5^{(1)}$ | 0 | 0.578 | 5.291 | 9.583 | 0.730 | 25.818 |
| $\Gamma_3$ | 0 | 2.000 | 0.182 | 0 | 25.818 | 0 |

TABLE III. Energies and wave functions $|n\rangle$ in terms of the states $|S_z\rangle$ for $Tb^{3+}$ ions ($S=6$) in the crystal field and molecular field appropriate to TbSb (model A).

| Energy of level, $E_n$ (THz) | Transition frequency, $\nu_n$ (THz) | | | | | | |
|---|---|---|---|---|---|---|---|
| | | $a$ | $\|6\rangle$ | $\|3\rangle$ | $\|0\rangle$ | $\|-3\rangle$ | |
| | | $b$ | $\|5\rangle$ | $\|2\rangle$ | $\|-1\rangle$ | $\|-4\rangle$ | |
| | | $c$ | $\|4\rangle$ | $\|1\rangle$ | $\|-2\rangle$ | $\|-5\rangle$ | $\|-6\rangle$ |
| −1.994 | 0 | $a$ | 0.925 | −0.353 | 0.139 | 0.027 | 0.006 |
| −1.315 | 0.679 | $b$ | 0.711 | −0.686 | 0.149 | 0.042 | |
| −1.190 | 0.804 | $c$ | −0.594 | 0.794 | 0.122 | 0.038 | |
| −0.957 | 1.038 | $a$ | −0.283 | −0.392 | 0.825 | 0.272 | 0.107 |
| −0.515 | 1.479 | $b$ | −0.222 | −0.011 | 0.904 | 0.366 | |
| −0.109 | 1.885 | $c$ | 0.232 | 0.020 | 0.858 | 0.458 | |
| 0.058 | 2.052 | $a$ | −0.197 | −0.615 | −0.127 | −0.479 | −0.581 |
| 0.308 | 2.302 | $b$ | 0.667 | 0.727 | 0.133 | 0.096 | |
| 0.359 | 2.353 | $a$ | 0.160 | 0.581 | 0.473 | −0.190 | −0.615 |
| 0.425 | 2.420 | $c$ | 0.770 | 0.606 | −0.154 | −0.128 | |
| 1.453 | 3.447 | $a$ | −0.015 | −0.083 | −0.245 | 0.813 | −0.522 |
| 1.678 | 3.672 | $b$ | 0.014 | 0.040 | 0.378 | −0.925 | |
| 1.799 | 3.793 | $c$ | 0.017 | 0.044 | −0.474 | 0.879 | |

$\vec{Q}$ in the $(1\bar{1}0)$ plane, but for certain directions and points of high symmetry there are fewer distinct magnon wave vectors.

### B. Equipment and sample

The experiment was carried out using the triple-axis crystal spectrometer at the C5 experimental facility of the NRU reactor, Chalk River. The constant-momentum-transfer (constant-$\vec{Q}$) mode of operation[23] was used throughout with variable incident-neutron frequency and with fixed scattered-neutron frequency $\nu' = 3.00$ THz in preliminary scans and 2.06 THz in later scans. A pyrolytic-graphite analyzing crystal [(002) plane] was used in conjunction with a squeezed germanium[24] monochromating crystal [(111) plane]. The specimen consisted of two single crystals of TbSb aligned so as to have identical crystallographic orientations with a $[1\bar{1}0]$ axis normal to the scattering plane. The total volume of the specimen was only 0.06 $cm^3$. This severe disadvantage in size was offset to some extent by the large magnetic scattering cross section for a $Tb^{3+}$ ion. The sample was placed in a helium cryostat and the temperature was measured and controlled by Ge and Pt resistance thermometers operating in conjunction with electrical heaters.

### C. Experimental results at 4.4 K

Examples of the distributions of neutrons scattered by the magnetic excitations in TbSb in various constant-$\vec{Q}$ scans are shown in Fig. 3. The time taken to collect each data point was about 30 min. In general, each peak contains contributions from four modes originating in the four domains, but these are experimentally unresolved since their frequencies are spaced typically by a few hundredths of a THz. At $(\frac{3}{4}, \frac{3}{4}, \frac{3}{4})$ and $(\frac{1}{2}, \frac{1}{2}, \frac{1}{2})$ single peaks which correspond to transitions from the ground to the first excited state (Fig. 1) were observed. At (110) two peaks are evident and these correspond to transitions from the ground state to the first and second excited states. Calculations of the spin-wave structure factors using the fitted exchange and crystal-field parameters indicate that the spin-wave intensity at (110) should be about half that at $(\frac{1}{2}, \frac{1}{2}, \frac{1}{2})$, in qualitative agreement with experiment. The calculations also indicate that two distinct groups should be observed at (001). In the measurements the lower peak was not observed although there is additional scattering in the expected range, 0.5–0.6 THz.

In the scan at (0.2, 0.2, 1.2) only one peak is observed although the analysis suggests that the first two branches of the dispersion relation should have

TABLE IV. Values of $\langle n|S_\alpha|0\rangle$ for model A. $\alpha$ stands for plus, minus, or $z$, and $n$ labels the states in order of increasing energy.

| $n$ | $\langle n\|S_+\|0\rangle$ | $\langle n\|S_-\|0\rangle$ | $\langle n\|S_z\|0\rangle$ | $\langle n\|S_z\|n\rangle$ |
|---|---|---|---|---|
| 0 | | | 5.503 | 5.503 |
| 1 | | 3.870 | | 3.439 |
| 2 | 1.886 | | | 2.007 |
| 3 | | | −1.179 | 0.651 |
| 4 | | 0.183 | | −1.106 |
| 5 | −0.280 | | | −2.304 |
| 6 | | | −0.383 | −1.348 |
| 7 | | 0.735 | | 3.224 |
| 8 | | | 0.309 | −1.270 |
| 9 | −0.966 | | | 2.603 |
| 10 | | | −0.042 | −3.597 |
| 11 | | 0.164 | | −3.561 |
| 12 | −0.051 | | | −4.312 |

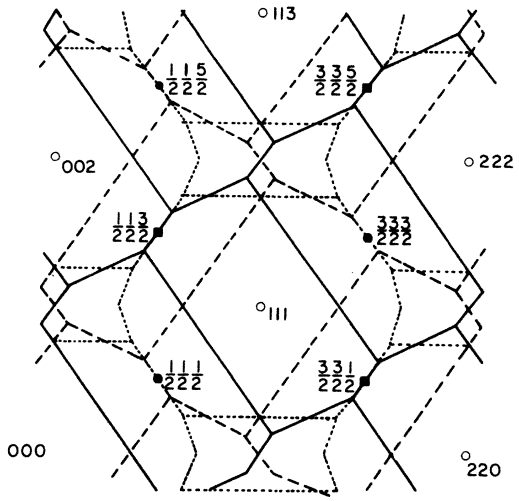


FIG. 2. Intersections of the magnetic Brillouin zones for domains having spin directions along [111] (solid lines), $[\bar{1}\bar{1}1]$ (long dashes), and $[\bar{1}11]$ and $[1\bar{1}1]$ (short dashes) with the $(1\bar{1}0)$ plane of the reciprocal lattice. Nuclear and magnetic reciprocal-lattice points are indicated by open and closed circles, respectively. Closed squares indicate the additional magnetic Bragg reflections observed because of the multidomain structure. All peaks are indexed on the basis of the chemical unit cell.

approximately equal intensity and frequencies of 0.68 and 0.83 THz. Both branches probably contribute to the peak since the full width at half-maximum (FWHM) is at least as large as the 0.17-THz FWHM observed in the incoherent elastic scattering from vanadium when $\nu' = 2.06$ THz.

The results are summarized in Fig. 4. Only those peaks where the scattering originates from a single branch of the dispersion relation were used in constructing Fig. 4. Where two peaks were observed in a constant-$\vec{Q}$ scan, e.g., at (110), two points appear in Fig. 4. The errors assigned to the frequencies are $\approx 10\%$ of the FWHM in the case of well-defined intense peaks and somewhat larger in cases where the peaks are very weak.

The most comprehensive measurements were made along [111] directions at several locations in reciprocal space with resolution corresponding to $\nu' = 2.06$ THz. The scans along [001] and [110] directions were made with $\nu' = 3.00$ THz and consequently the error limits are somewhat larger than for the [111] direction. At (0.5, 0.5, 1.3) and (1.5, 1.5, 1.3) the observed frequencies are $0.63 \pm 0.03$ and $0.57 \pm 0.03$ THz, respectively. According to the calculations the domain-averaged frequencies should be almost identical at these positions. In fitting procedures, such points were given equal weight, and the theoretical curve comes between the pairs of experimental points.

In addition to the magnetic scattering below 1 THz there is evidence of weak magnetic scattering at 4.4 K at about 2.5 THz as shown in Fig. 3 at (0.65, 0.65, 1.65). This scattering probably corresponds to transitions between the ground state and the seventh and ninth excited states. Arrows on Fig. 3 show the frequencies of these transitions calculated from the best exchange and crystal-field parameters, and the relevant matrix elements are given in Fig. 1.

### D. Temperature dependence of the excitations

Measurements of the scattering as a function of temperature confirm the magnetic character of the associated modes. Figure 5 shows the scattering at (1.45, 1.45, 1.45), which is near a zone center, for 4.4, 10.0, 11.5, and 13.0 K in the antiferromagnetic phase and 20.2, 28.0, and 38.1 K in the paramagnetic phase. In Fig. 5 the nuclear incoherent elastic scattering and the flat background scattering were obtained from the scan at 4.4 K and subtracted from the scans at higher temperatures. The important features are the movement

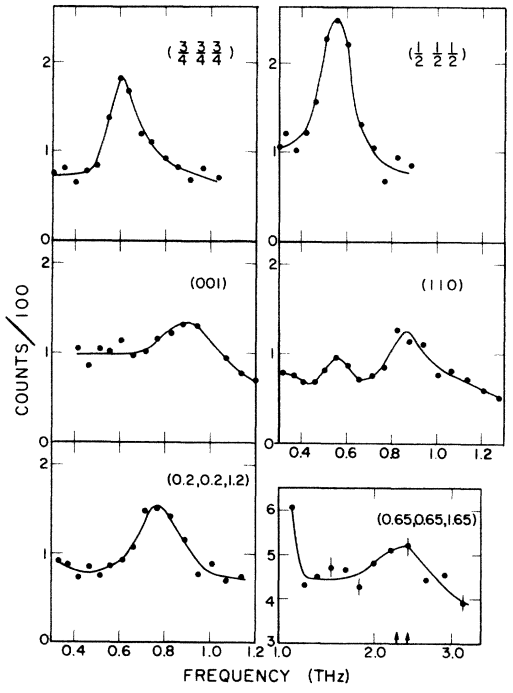


FIG. 3. Typical scattered-neutron distributions for TbSb at 4.4 K. Each distribution is labeled with the value of the wave-vector transfer $\vec{Q}$ (in units of $2\pi/a$) at which the measurement was made. All distributions are normalized to the same number of counts in the incident-beam monitor with the exception of the distribution at (0.65, 0.65, 1.65).

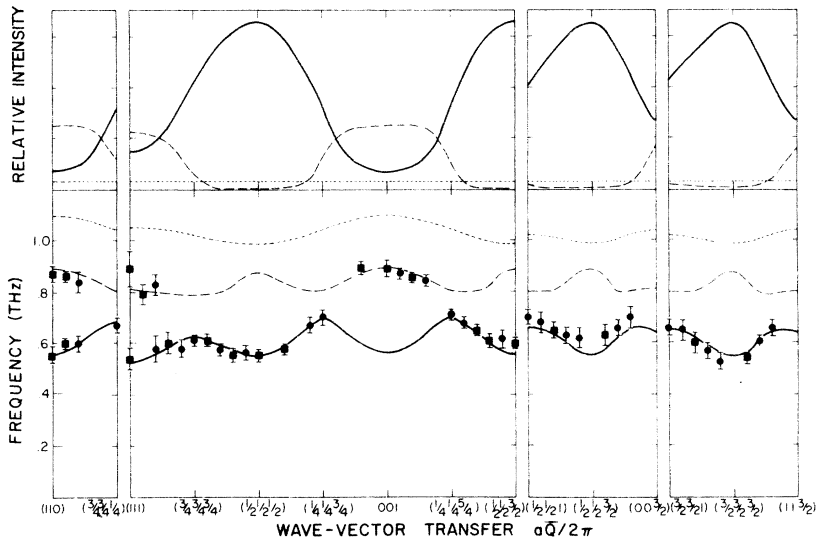


FIG. 4. Frequency and intensity versus wave-vector transfer for the magnetic excitations in TbSb at 4.4 K. The curves are averages over the four domain frequencies and intensities for the first three branches of the dispersion relation determined from model A. Squares indicate those data points used in model B (see text).

of the peak observed initially at 0.54 THz to lower frequencies as the temperature is raised, and the growth of the zero-frequency response. At 13.0 K the latter, similar in form to critical scattering, is much more intense than the shoulder observed near 0.3 THz, which presumably represents the renormalized excitations associated with the lowest branch. Above $T_N$ the response has the form of a smooth distribution of intensity extending to about 0.6 THz with no evidence of a shoulder.

Near a zone boundary the results [Fig. 6(a)] are qualitatively different from those near the zone center (Fig. 5). Above $T_N$ there is a shoulder in the scattering near 0.3 THz which becomes weaker as the temperature is raised. This shoulder is attributed to the $\Gamma_1 \rightarrow \Gamma_4$ and $\Gamma_4 \rightarrow \Gamma_5^{(2)}$ transitions which, in the limit of zero molecular field, occur at 0.28 and 0.32 THz, respectively. The population of the $\Gamma_1$ and $\Gamma_4$ levels decreases between 20.8 and 38.1 K because of the increasing population of higher states and this can account for the observed fall in intensity. The broad distribution of weak scattering between 1 and 2 THz observed at 103 K [Fig. 6(b)] is attributed to the $\Gamma_5^{(2)} \rightarrow \Gamma_2$, $\Gamma_5^{(2)} \rightarrow \Gamma_5^{(1)}$, and $\Gamma_4 \rightarrow \Gamma_3$ transitions (see Table V).

## III. THEORY

### A. Single-ion Hamiltonian

For TbSb the simplest Hamiltonian which incorporates both exchange and crystal-field effects is

$$\mathcal{H} = \sum_{j,k} \sum_{j',k'} J\begin{pmatrix} j & j' \\ k & k' \end{pmatrix} \vec{S}(j,k) \cdot \vec{S}(j',k') + \mathcal{H}_{cf} . \qquad (1)$$

Here $j$ is an index which labels the unit cell, $k$ labels the magnetic ions within a cell ($k = 1$ or 2 for a two-sublattice antiferromagnet), and $\vec{S}$ is the total spin plus orbital angular momentum. $\mathcal{H}_{cf}$ describes the octahedral crystal field with rhombohedral distortion. Equation (1) may be written in two parts: the single-ion part $\mathcal{H}^{(1)}$ contains the crystal-field contribution and that part of the exchange which may be written in terms of a molec-

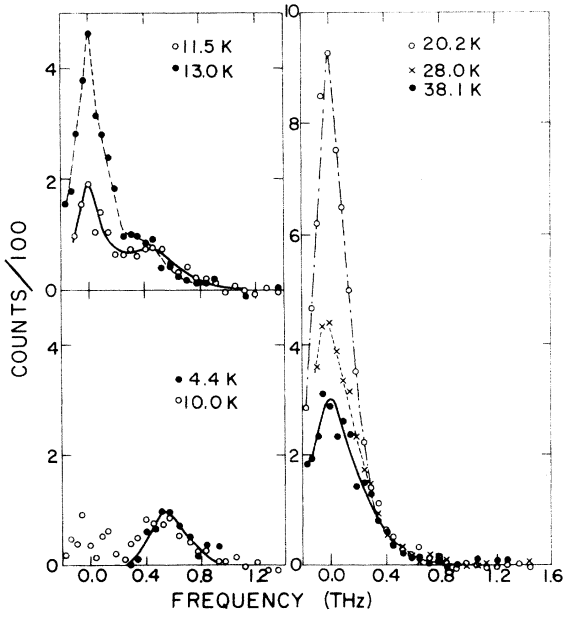


FIG. 5. Neutron scattering at (1.45, 1.45, 1.45), which is close to a magnetic reciprocal-lattice point, as a function of temperature above and below $T_N$. The nuclear incoherent scattering and a flat background were determined from the scan at 4.4 K and subtracted from the scans at higher temperatures. The curves are simply a guide to the eye.

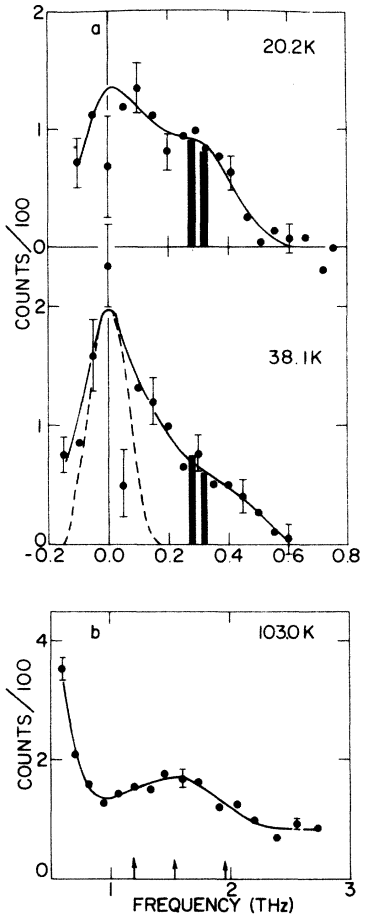


FIG. 6. (a) Scattering in the nonordered phase at $(\frac{3}{4}, \frac{3}{4}, \frac{3}{4})$ at 20.8 and 38.1 K. Background and incoherent-elastic-scattering contributions have been subtracted and the distributions have been normalized to the same number of counts in the incident-beam monitor. The vertical bars indicate the frequencies of the $\Gamma_1$ to $\Gamma_4$ and $\Gamma_4$ to $\Gamma_5^{(2)}$ transitions. The dashed curve shows the experimental resolution. (b) Weak scattering in the nonordered phase which corresponds to transitions between several excited states (see Sec. II D) indicated by arrows.

ular field, and the interion part $\mathcal{H}^{(2)}$ contains the remaining exchange contributions. For an ion on sublattice $k$ the single-ion part $\mathcal{H}^{(1)}$, taking the crystal-field $z$ axis along the [111] direction, is a sum of terms for each site of the form

$$-\tfrac{2}{3}B_4^0[O_4^0 - 20\sqrt{2}\,O_4^3] + \tfrac{16}{9}B_6^0[O_6^0 + \tfrac{35}{4}\sqrt{2}\,O_6^3 + \tfrac{77}{8}O_6^6] + B_2^0\,O_2^0 + (-1)^k H_Z S_Z \,, \quad (2)$$

where $B_4^0$ and $B_6^0$ are cubic-crystal-field parameters and the $O_n^m$ are operator equivalents with matrix elements tabulated by Hutchings.[25] The $B_2^0$ term allows for a rhombohedral distortion of the unit cell. The contribution of the interion terms is

$$\mathcal{H}^{(2)} = \sum_{j,k}\sum_{j',k'} J\begin{pmatrix} j & j' \\ k & k' \end{pmatrix} \vec{S}(j,k)\cdot\vec{S}(j',k') - \sum_{j,k}(-1)^k H_Z S_Z(j,k) \,. \quad (3)$$

The molecular field is directed along the [111] ordering direction of TbSb and is given by

$$H_Z = 2\sum_r Z_r J_r \langle S_Z\rangle \,, \quad (4)$$

where $J_r$ and $Z_r$ are the exchange constant and coordination number for the $r$th neighbor, and $\langle S_Z\rangle$ is the thermal average of $S_Z$ over all the states. $\mathcal{H}^{(1)}$ describes the effect of the mixing of excited-state wave functions into the ground-state wave function by the molecular field. The molecular-field energies $E_n$ and wave functions $|n\rangle$ ($n=0$ to 12) have been obtained by diagonalizing $\mathcal{H}^{(1)}$ (13 $\times$13) and the behavior of the energies is shown in Fig. 1. The wave functions $|n\rangle$ for zero molecular field and for the molecular field corresponding to the best-fitted exchange and crystal-field parameters (model A) are tabulated in Tables I and III; they differ markedly in the two cases. The matrix elements for transitions between the ground state and the excited states are given in Tables II and IV. In the presence of a molecular field the symmetry labels of Table II are no longer appropriate, so the levels are listed in order of increasing energy in Table IV. Note that the matrix elements in Table II are defined in terms of the levels and matrix elements used in the rest of this paper as

$$|\langle\Gamma_i|\,S_\alpha\,|\,\Gamma_j\rangle|^2 \equiv \sum_{m,n}|\langle m(\Gamma_i)|\,S_\alpha\,|\,n(\Gamma_j)\rangle|^2$$

for $\alpha = +, -, z$, where $m, n$ run over the degenerate levels of the two crystal field states. The other result necessary to relate to the matrix elements of this paper is that

$$|\langle\Gamma_i|\,S_+\,|\,\Gamma_j\rangle|^2 = |\langle\Gamma_i|\,S_-\,|\,\Gamma_j\rangle|^2 = 2\,|\langle\Gamma_i|\,S_z\,|\,\Gamma_i\rangle|^2$$

in the disordered phase.

### B. Spin waves

The interion term $\mathcal{H}^{(2)}$ couples together the single-ion excitations described in Sec. III A, and gives rise to the spin waves of the antiferromagnetic state. In this paper $\mathcal{H}^{(2)}$ is treated by the pseudoboson method developed by Grover[22] which is valid when the ground state alone is populated. Operators $a^\dagger(jkn)$ are defined which excite the $j$th ion on the $k$th sublattice from the ground state $|0\rangle$ to the excited state $|n\rangle$ with transition frequency $\nu_n = (E_n - E_0)/h$. A complete description of the components of the spin operator $S_\alpha(jk)$ ($\alpha = +, -,$ or $z$) within the ground multiplet is then given by

TABLE V. Relative intensities of the excitations corresponding to allowed transitions between the states of the $^7F_6$ multiplet of the $Tb^{3+}$ ion in zero molecular field (model A).

| $\Delta\nu$ (THz) | Transition | Relative intensity 0 K | 16.0 K | 20.2 K | 28.0 K | 38.1 K | 300 K |
|---|---|---|---|---|---|---|---|
| 0 | $\Gamma_4 \rightarrow \Gamma_4$ | 0 | 0.08 | 0.08 | 0.08 | 0.07 | 0.05 |
| 0 | $\Gamma_5^{(2)} \rightarrow \Gamma_5^{(2)}$ | 0 | 0.43 | 0.53 | 0.63 | 0.68 | 0.67 |
| 0 | $\Gamma_5^{(1)} \rightarrow \Gamma_5^{(1)}$ | 0 | 0.00 | 0.00 | 0.01 | 0.01 | 0.04 |
| 0.11 | $\Gamma_5^{(1)} \rightarrow \Gamma_3$ | 0 | 0.03 | 0.03 | 0.15 | 0.36 | 1.16 |
| 0.28 | $\Gamma_1 \rightarrow \Gamma_4$ | 14.00 | 4.96 | 4.24 | 3.39 | 2.83 | 1.71 |
| 0.32 | $\Gamma_4 \rightarrow \Gamma_5^{(2)}$ | 0 | 3.84 | 3.87 | 3.77 | 3.54 | 2.66 |
| 0.34 | $\Gamma_2 \rightarrow \Gamma_5^{(1)}$ | 0 | 0.02 | 0.04 | 0.11 | 0.20 | 0.51 |
| 1.19 | $\Gamma_5^{(2)} \rightarrow \Gamma_2$ | 0 | 0.27 | 0.32 | 0.39 | 0.42 | 0.41 |
| 1.53 | $\Gamma_5^{(2)} \rightarrow \Gamma_5^{(1)}$ | 0 | 0.32 | 0.39 | 0.47 | 0.50 | 0.49 |
| 1.64 | $\Gamma_5^{(2)} \rightarrow \Gamma_3$ | 0 | 0.01 | 0.01 | 0.01 | 0.02 | 0.02 |
| 1.85 | $\Gamma_4 \rightarrow \Gamma_5^{(1)}$ | 0 | 0.09 | 0.09 | 0.09 | 0.08 | 0.06 |
| 1.96 | $\Gamma_4 \rightarrow \Gamma_3$ | 0 | 0.31 | 0.31 | 0.30 | 0.28 | 0.22 |

$$S_+(jk) = \sum_n \left[ S_{+n0}\, a^\dagger(jkn) + S_{+0n}\, a(jkn) \right] , \tag{5}$$

$$S_z(jk) = S_{z00} + \sum_n S_{zn0} \left[ a^\dagger(jkn) + a(jkn) \right] + \sum_n (S_{znn} - S_{z00})\, a^\dagger(jkn)\, a(jkn) . \tag{6}$$

The matrix elements $S_{\alpha n0}$ for the up-spin sublattice, $k=1$, are the elements $\langle n \mid S_\alpha \mid 0 \rangle$ in a molecular field listed in Table IV. The matrix elements for the down-spin sublattice, $k=2$, can be obtained by changing $S_z$ to $-S_z$ and $S_+$ to $S_-$. The single-ion Hamiltonian is diagonal in the pseudoboson representation,

$$\mathcal{H}^{(1)} = \sum_n \sum_{jk} h\nu_n\, a^\dagger(jkn)\, a(jkn) . \tag{7}$$

The interion Hamiltonian is also transformed by Eqs. (5) and (6) and only those terms which are quadratic in pseudoboson operators are retained. The total Hamiltonian is transformed to reciprocal space and finally diagonalized to yield for each wave vector a set of excitation frequencies $\nu(\vec{q}s)$ and eigenvectors $u(\vec{q}s, kn)$, $v(\vec{q}s, kn)$, where $s$ is the branch index which runs from 1 to 24. The eigenvectors specify the fraction of spin-wave wave function contributed by the creation or destruction of a single-ion state; the spin-wave annihilation operator is then

$$\alpha(\vec{q}s) = \sum_{kn} \left[ u(\vec{q}s, kn)\, a(\vec{q}s, kn) - v(\vec{q}s, kn)\, a^\dagger(-\vec{q}s, kn) \right] . \tag{8}$$

A description of the pseudoboson method in a form applicable to a variety of systems including TbSb is given by Buyers *et al.*[26]

The branches of the dispersion relation may be divided into those involving $S_+$ or $S_-$ operators which are doubly degenerate and those involving $S_z$ which are nondegenerate and exhibit the so-called Davydov splitting.

### C. One-magnon cross section

In order to compare with experiment it is necessary to evaluate the frequency averaged over the domains, since this is what is measured in a multidomain crystal. This involves calculating the differential neutron scattering cross section per cell for magnetic scattering from each domain of the crystal. For a given domain the cross section for the spin wave with wave vector $\vec{q}$ is

$$S(\vec{Q}, \nu) = \left( \frac{\gamma e^2}{2mc^2} \right)^2 f^2(\vec{Q}) \sum_s \mid F(\vec{q}s) \mid^2 \{ \delta[\nu + \nu(\vec{q}s)]\, n(\vec{q}s) + \delta[\nu - \nu(\vec{q}s)]\, [n(\vec{q}s) + 1] \} \sum_{\vec{\tau}} \Delta(\vec{Q} - \vec{q} - \vec{\tau}) , \tag{9}$$

where $\vec{\tau}$ is a vector of the magnetic reciprocal lattice, $\vec{Q}$ is the wave-vector transfer, $f(\vec{Q})$ is an atomic form factor, $\nu(\vec{q}s)$ is the frequency of the $s$th branch of the dispersion relation, and $n(\vec{q}s)$ is the Bose occupation number. In an experiment at constant $\vec{Q}$ there are contributions to the scattering from the four domains associated with the four spin directions of the form $[HKL]$, viz., $[111]$, $[\bar{1}\bar{1}1]$, $[\bar{1}11]$, and $[1\bar{1}1]$. Each domain can be generated by rotating the $[111]$ domain about the $[001]$ axis by a rotation matrix $\vec{T}_{HKL}$. The results for the spin-wave frequency and intensity are correctly obtained if we rotate $\vec{Q}$ by $\vec{T}^{-1}_{HKL}$ so that the orientation of the rotated wave vector $\vec{T}^{-1}_{HKL}\,\vec{Q}$ to the $[111]$-domain spin direction is maintained. In this way all reduced wave vectors are referred to a fixed $[111]$ domain. The appropriate domain wave

vector is given by

$$\vec{q}_d = \vec{T}^{-1}_{HKL}\,\vec{Q} - \vec{\tau}\,, \tag{10}$$

where $\vec{\tau}$ is a reciprocal-lattice vector of the [111] domain. The corresponding structure factor is then given by

$$|F(\vec{q}_d s)|^2 = \tfrac{2}{3} g\mu_B (1 - HK\hat{Q}_x\hat{Q}_y - KL\,\hat{Q}_y\hat{Q}_z - LH\hat{Q}_z\hat{Q}_x)\left|\sum_n S_{zn0}(u_{s1n} - u_{s2n} + v_{s1n} - v_{s2n})\right|^2 \tag{11}$$

for the $S_z$ modes, and

$$|F(\vec{q}_d s)|^2 = \tfrac{1}{6} g\mu_B (2 + HK\hat{Q}_x\hat{Q}_y + KL\,\hat{Q}_y\hat{Q}_z + LH\hat{Q}_z\hat{Q}_x)\left(\left|\sum_n S_{+n0}(v_{s1n} \pm u_{s2n}) + \sum_n S_{-n0}(u_{s1n} \pm v_{s2n})\right|^2 + \left|\sum_n S_{+n0}(u_{s1n} \pm v_{s2n}) + \sum_n S_{-n0}(v_{s1n} \pm u_{s2n})\right|^2\right) \tag{12}$$

for the $S_+$ and $S_-$ modes. Symbols such as $u_{skn}$ are short for $u(\vec{q}_d s, kn)$. The upper signs apply in zones containing nuclear reciprocal-lattice points and the lower signs apply in zones containing magnetic reciprocal-lattice points. The components of $\hat{\vec{Q}}$ are defined with respect to the Cartesian axes of the cubic crystallographic cell, while the axes for the spins are the crystal-field axes with $z$ along the [111] magnetization direction. The domain-averaged frequency which should be directly comparable with experiment is then given by

$$\bar{\nu}(\vec{Q}s) = \sum_{d=1}^{4} |F(\vec{q}_d s)|^2\, \nu(\vec{q}_d s) \Big/ \sum_{d=1}^{4} |F(\vec{q}_d s)|^2\,. \tag{13}$$

### D. Temperature dependence of the intensities of the crystal-field excitations

In order to have a qualitative description of the temperature dependence of the intensities observed in the paramagnetic phase it is useful to evaluate the magnetic scattering in the limit of vanishing exchange interaction. This is proportional to[21]

$$2\sum_{i,j} \rho_j |\langle \Gamma_i | S_z | \Gamma_j \rangle|^2\, \delta(E_i - E_j - h\nu)\,, \tag{14}$$

where $\rho_j$ is the fractional population of the $j$th state at temperature $T$ and $E_j$ is its energy. The matrix elements involved have already been given in Table II. The relative intensities of the allowed transitions at a number of temperatures, obtained using the best-fit parameters to determine the crystal-field-only transitions, have been tabulated in Table V. Since the exchange contribution is important in TbSb, the above expression provides an incomplete description of the situation, but it does provide a basis for understanding the shape and temperature dependence of the scattering at 0.3 THz and the presence of weak scattering near 1.5 THz. This is shown in Fig. 6(a), where the calculated intensities of Table V, given by the heights of the vertical bars at the transition frequencies, are seen to be in reasonable agreement with experiment.

## IV. ANALYSIS OF RESULTS

The crystal-field parameters ($B_2^0$, $B_4^0$, $B_6^0$) and the exchange parameters ($J_1$, $J_2$) for TbSb can be obtained from the observed spin-wave frequencies and intensities using the theory of Sec. III. The dominant antiferromagnetic exchange, $J_2$, is between a Tb ion and its six second-nearest neighbors on the opposite sublattice. The nearest-neighbor interaction $J_1$ is between a Tb ion and its 12 nearest neighbors, six on the same sublattice and six on the opposite sublattice. Various methods of analysis were tested but we shall only discuss the two most satisfactory models, referred to as models A and B. A reasonably good representation of the observed frequencies was first obtained by varying the parameters $B_4^0$, $J_1$, and $J_2$ on an intuitive basis, starting from the parameters given by Cooper and Vogt.[12] The structure factors $|F(\vec{q}_d s)|^2$ for the four domains were then calculated. They were held constant in subsequent analysis since they should be insensitive to small changes in frequencies, as was later confirmed with the final parameters of model A.

In model A, $J_1$, $J_2$, and $B_4^0$ were obtained by least-squares fitting to the experimental frequencies in Fig. 4. An excellent description of the lowest two branches of the dispersion relation (solid and long-dash curves in Fig. 4) was obtained with the crystal-field and exchange parameters given in Table VI (model A). The calculated dispersion relation for the third branch is also shown in Fig. 4, but no experimental points belonging to this weak branch were obtained. Note that if $J_1$ is held equal to zero, the model predicts no difference between the frequencies at $(\frac{3}{4}, \frac{3}{4}, \frac{3}{4})$ and $(\frac{1}{4}, \frac{1}{4}, \frac{5}{4})$, whereas experiment shows that these frequencies are $0.61 \pm 0.02$ and $0.71 \pm 0.02$ THz. $J_1$ is thus very sensitive to this rather small difference. The

TABLE VI. Crystal-field and exchange parameters for TbSb obtained from analysis of experimental results.

| | | $B_4^0$ (THz) | $J_1$ (THz) | $J_2$ (THz) | $B_2^0$ (THz) |
|---|---|---|---|---|---|
| Present work | model A | $(1.55 \pm 0.11) \times 10^{-4}$ | $(-1.03 \pm 0.15) \times 10^{-3}$ | $(2.92 \pm 0.07) \times 10^{-3}$ | 0 |
| | model B | $1.38 \times 10^{-4}$ | $(-0.39 \pm 0.12) \times 10^{-3}$ | $(2.64 \pm 0.10) \times 10^{-3}$ | $-(0.84 \pm 0.36) \times 10^{-3}$ |
| Cooper and Vogt[a] | | $1.38 \times 10^{-4}$ | | $1.83 \times 10^{-3}$ | |
| Busch[b] | | | $2.08 \times 10^{-3}$ | $7.10 \times 10^{-3}$ | |
| Point-ion model[c] | | $2.2 \times 10^{-4}$ | | | $-4.8 \times 10^{-3}$ |

[a]In paramagnetic-susceptibility measurements such as those of Cooper and Vogt the value of the combination $(J_2 + 2J_1 + \cdots)$ is determined and it is this value which is given in the column for $J_2$.
[b]Reference 27.
[c]Derived from x-ray measurements described in Ref. 20.

effect of allowing the sixth-order crystal-field term $B_6^0$ to vary in the fitting procedure was tested. $B_6^0$ was found to be $(-0.8 \pm 2.6) \times 10^{-8}$ THz while the other parameters departed from the values in Table VI by less than 2%. In further analyses $B_6^0$ was therefore set equal to zero. The effect of also fitting the frequency of the peak observed at (0.65, 0.65, 1.65) (Fig. 3) to the average of the frequencies of the seventh and ninth branches was investigated and again negligible change from model A was found. We conclude that model A gives a good description of the higher transitions as well as the lowest two exciton branches.

In the second model, B, the parameters were obtained by fitting ten selected frequencies (designated by filled squares in Fig. 4) as well as the Néel temperature and the measured susceptibility[27] of TbSb at 20 K. The latter two quantities were calculated within the molecular-field approximation and are therefore not determined to better than $\approx 10\%$. In addition to the parameters of model A, this model contained a crystal-field term, $B_2^0$, corresponding to a rhombohedral distortion of the crystal structure. In the presence of a rhombohedral distortion the first-neighbor exchange to the opposite sublattice decreases while that to the same sublattice increases as given by $J_1(\text{diff}) = J_1(1 - G)$ and $J_1(\text{same}) = J_1(1 + G)$, where $G$ depends on the magnitude of the distortion and the rate of change of exchange with distance. Assuming a value of $d(\ln | J |)/d(\ln r)$ of $-21$ as found in measurements[28] of a similar distortion in MnO, $G$ was found to be $+0.02$ using the measured[20] distortion and fixed at this value in the fitting. $B_4^0$ was fixed at the value obtained by Cooper and Vogt, [12] and $B_2^0$, $J_1$, and $J_2$ were treated as variable parameters in the fitting procedure. The values thus obtained are given in Table VI.

The dispersion curves and intensities for multidomain TbSb obtained from the parameters of model A are given in Fig. 4, and the frequencies for the lowest two branches are seen to be in good agreement with experiment. Various other predictions of model A are given in Fig. 1 and Tables I and III–V. The predictions of models A and B for the low-frequency part of the dispersion relation for single-domain TbSb in high-symmetry directions are shown in Fig. 7, and the frequencies for the higher-frequency branches, which are almost wave-vector independent, are listed in Table VII.

The fitting error for model A (0.9) is somewhat smaller than for model B (1.4), but the frequencies and intensities calculated from the two models are not very different and it is difficult to decide which is the better model.

One general feature that emerges from both models is that the lowest branch has maximum intensity in zones containing magnetic reciprocal-lattice points while the second branch has maximum intensity in zones containing nuclear reciprocal-lattice points. The experimental results confirm this behavior. Both models predict that the first and second branches have comparable intensities near the zone boundary in zones containing

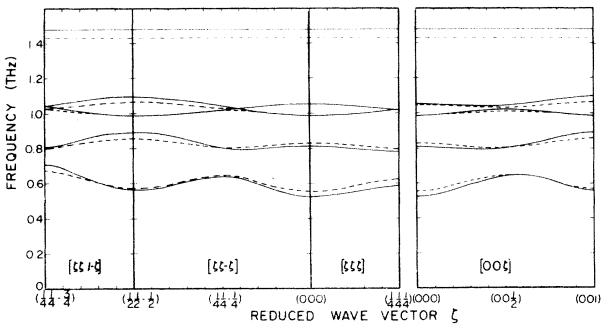


FIG. 7. Low-frequency part of the dispersion relation for single-domain TbSb at 0 K in major symmetry directions calculated from model A (solid line) and model B (dashed line). The frequencies of the flat higher-frequency branches are listed in Table VII.

TABLE VII. Frequencies of the flat upper branches of the dispersion relation for models A and B. See also Fig. 7.

| $\nu$ (THz) A | $\nu$ (THz) B |
|---|---|
| 1.479 | 1.430 |
| 1.885 | 1.786 |
| 2.050 | 1.900 |
| 2.301 | 2.109 |
| 2.353 | 2.173 |
| 2.419 | 2.226 |
| 3.447 | 3.166 |
| 3.672 | 3.370 |
| 3.793 | 3.467 |

nuclear reciprocal-lattice points. The third branch has a much lower intensity than that of the lowest two branches, as shown in Fig. 4, and was not observed in the experiment.

## V. DISCUSSION

### A. Low-temperature excitations

The models developed in Sec. IV give an excellent description of the low-lying excitations in TbSb. For model A the rms error is essentially the same as the average error (~ 3%) on each experimental point. Prior to these neutron scattering measurements the best available parameters for TbSb were those of Cooper and Vogt,[12] which give a set of frequencies, calculated within the pseudoboson model, 30% below those observed experimentally.

The values of $B_4^0$ and the antiferromagnetic exchange $J_2$ are accurately determined and differ little between models A and B, while $B_6^0$ is zero within error. The near-neighbor exchange $J_1$ is not so accurately determined, however, although both models predict that it is ferromagnetic in sign. This is because $J_1$ depends on the small frequency differences observed near zone boundaries such as at the wave vectors of Table VIII. Model B was introduced in order to obtain a more consistent description of the observed susceptibility and Néel temperature as well as the neutron data. Table VIII shows to what extent this was successful. The larger fitting error of model B is probably because molecular-field theory is incapable of giving an accurate value for the susceptibility and Néel temperature, although this was allowed for to some extent by assigning large errors to these data points in the fitting procedure. To fit the Néel temperature and the susceptibility in model B, $J_2$ is decreased from the model-A value in order to reproduce $T_N$, while $J_2 + 2J_1$ is increased in order to reproduce the susceptibility. Since $J_2 > 0$ and $J_1 < 0$ this can only be done by reducing the magnitude of $J_1$.

In Table VI the exchange and crystal-field parameters deduced from the present work are compared with previous work[12,29] and with estimates from the point-charge model of the crystal field with effective charge $-3$ on the ligand sites using values of $\langle r^n \rangle$ taken from Kasuya.[30] The experimental value of $B_4^0$ suggests that the effective charge on the ligand sites is approximately $-2$, in agreement with studies of other pnictides.[17] A negative rhombohedral-distortion term $B_2^0$ as found for model B tends to enhance the induced moment at a given molecular field and acts to stabilize the magnetism. The value of $B_2^0$ found is, however, six times smaller than the prediction of the point-charge model on the basis of the observed rhombohedral distortion.[20]

The ratio $\eta = 24 J_2 (S_{z20})^2/\Delta$, where $\Delta$ is the splitting between the ground singlet and the lowest triplet, is 3.5 for model A and 3.7 for model B. Both are more than three times the critical ratio of unity[4] for ordering to occur at 0 K in the molecular-field model. Thus TbSb, although an induced antiferromagnet, orders strongly. Since TbSb is a type-II antiferromagnet its magnetic structure is stable[31] within the molecular-field model only for a certain range of the ratio $J_2/J_1$. For the value of $J_2$ found in model A, $J_1$ must satisfy $6\times10^{-3} > J_1 > -3\times10^{-3}$ THz, which it clearly does. Similarly for model B the condition for the stability of the type-II antiferromagnetic structure is satisfied by the exchange parameters.

It is worthwhile making some comments on the appropriateness of the singlet-triplet model for describing the low-temperature spectrum of TbSb apart from its obvious inability to describe the weak scattering, for instance to the seventh and ninth levels. The wave function for the lowest state in the molecular field appropriate to model A is given in Table III. If this wave function is written as a linear combination of states of the same symmetry in the nonordered phase it is found that

$$|0\rangle = 0.602\,|\Gamma_1\rangle + 0.686\,|\Gamma_{4b}\rangle + 0.401\,|\Gamma_{5b}^{(2)}\rangle - 0.072\,|\Gamma_{3b}\rangle + 0.043\,|\Gamma_{5b}^{(1)}\rangle\,. \quad (15)$$

Thus it is clear that a major part of the wave function of the ground state comes from admixture of the states beyond the first triplet. The recent calculation of the excitation spectrum of TbSb by Hsieh and Blume[7] illustrates the difficulties the singlet-triplet model has in describing real systems.

As emphasized by Birgeneau[9] the model is incapable of producing the observed gap at $q = 0$ for any values of the parameters. This gap is large and has been directly observed in TbSb, unlike the

TABLE VIII. Comparison of calculated and experimental quantities for models A and B.

| | Model A | Model B | Experiment |
|---|---|---|---|
| $\bar{\nu}$ (THz) at $(\frac{3}{4},\frac{3}{4},\frac{3}{4})$, lowest branch | 0.62 | 0.64 | $0.61 \pm 0.02$ |
| $\bar{\nu}$ (THz) at $(\frac{1}{4},\frac{1}{4},\frac{5}{4})$, lowest branch | 0.70 | 0.67 | $0.71 \pm 0.02$ |
| $J_2 + 2J_1 + \cdots$ [a] (THz) | $(0.86 \pm 0.37) \times 10^{-3}$ | $(1.86 \pm 0.34) \times 10^{-3}$ | $1.83 \times 10^{-3}$ |
| Susceptibility[b] (emu mole$^{-1}$) at 20 K | 0.413 | 0.326 | 0.296 |
| Néel temperature[c] (K) | 22.0 | 20.2 | $14.9 \pm 0.2$ |
| Magnetization[d] $S_z$ | 5.51 | 5.58 | 5.45 |

[a] As determined from susceptibility measurements of $Tb_xY_{1-x}Sb$ alloys. Reference 12.
[b] Reference 27. Error used to determine the statistical weight in the fitting procedure was $\pm 5\%$.
[c] Error used to determine the statistical weight in the fitting procedure was $\pm 10\%$.
[d] Reference 1.

situation in $Pr_3Tl$, where measurements at $q = 0$ were not possible.[16] The finite energy gap at $q = 0$ is only obtained when higher states are included as in the present pseudoboson theory. Hsieh and Blume find fewer modes within the singlet-triplet than are expected on physical grounds. Apart from the longitudinal modes they show four transverse modes in their Fig. 17 instead of five. The fifth, which corresponds to the transition between the first and second excited states, is easily seen from Table III to have an appreciable dipole transition strength. It is absent in the model of Hsieh and Blume possibly because they have transformed to pseudo spin coordinates using crystal-field-only states where the transition is absent. The neglect of higher levels in treating the interion exchange does not allow the transition to appear as it should in the presence of an ordered moment. Note that for other systems in which the spin is in the [001] rather than the [111] direction this mode is indeed absent. Of the four transverse modes in their Fig. 17 at $T = 0$ those corresponding to transitions between excited states (e.g., $E_1$ and $E_2$) have zero magnetic dipole strength and are unobservable experimentally. Apart from their Goldstone mode $E_4$, the remaining observable mode $E_3$, which corresponds to the second branch of the dispersion relations, has a frequency of $\sim 1.5$ THz in contrast with the observed value $\sim 0.9$ THz (Fig. 4). Although we believe the qualitative differences between our experiment or theory and the Hsieh and Blume theory are serious, we attach less importance to the quantitative differences for they used a value of $J_2$ that was $2\frac{1}{2}$ times too large for TbSb.

### B. Excitations at higher temperatures

The temperature variation of the modes belonging to the lowest branch of the dispersion relation is observed to be quite rapid (see, e.g., Fig. 5). This behavior contrasts with that observed[16] for $Pr_3Tl$, which has a much smaller ratio of exchange to crystal field, and for which there is a very weak apparent temperature dependence. (The weak temperature dependence of the scattering can readily be explained by taking into account excitations between excited states of the ground multiplet.)[32] In TbSb the renormalization of the spin-wave frequency is greater because the relatively large ratio of exchange field to crystal field produces a significant change in the transition energy as $\langle S_z \rangle \to 0$. The most dramatic change in the scattering as the temperature is raised is the development of the scattering around $\nu = 0$. At least part of this response can be attributed to the excitations between excited states which are not considered in the pseudoboson model. For example, nearly-elastic transitions within the triplet have been found[33] to produce significant effects on the soft-mode behavior of $Pr_3Tl$.

There has been much discussion[8,9] on whether or not the transition in induced-moment systems is caused by a soft spin-wave mode. The presence of such a mode in TbSb is certainly consistent with our observations below the Néel temperature, but above $T_N$ there is no evidence for any well-defined excitation that could be called a soft mode. Observed instead is quasielastic scattering that peaks as $\vec{q} \to 0$ and $T \to T_N$. This is reminiscent of critical scattering and is similar to the scattering observed in systems such as the rare-earth metals[34] where the exchange energies are much larger than the crystal-field energies.

It might be argued that the increase in critical scattering as $T \to T_N$ is a result of a well-defined soft mode whose frequency is falling and which cannot be resolved with the finite instrumental resolution from other scattering in the low-energy range. The physics of TbSb, however, indicates (see Fig. 1) that the fluctuations above $T_N$ produce changes in the exchange part of the exciton fre-

quencies at least as large as the crystal-field energies themselves. Thus it seems unlikely that collective excitations can propagate through the crystal without being strongly damped. This suggests that the excitations, at least the long-wavelength low-lying ones, are overdamped at all temperatures above $T_N$. For the short-wavelength modes, e.g., those observed at $(\frac{3}{4}, \frac{3}{4}, \frac{3}{4})$, there is an indication [Fig. 6(b)] of a shoulder at 0.3 THz, suggesting that the damping is less important for these modes.

The behavior of TbSb differs from that of $Pr_3Tl$, where, because the exchange fluctuations are small compared with the crystal-field energies, well-defined modes can be observed above the ordering temperature. Although dynamical-susceptibility theory[33] gives a satisfactory description of the temperature dependence in $Pr_3Tl$, it is unlikely to do so for TbSb with its larger exchange. It remains an open and challenging problem to find a method of taking into account the effect of the exchange fluctuations on the spin-wave frequencies and lifetimes in a many-level system.

ACKNOWLEDGMENTS

The continuing interest of B. R. Cooper in this work is greatly appreciated as are several useful discussions. Valuable technical assistance was given by R. S. Campbell, A. Hewitt, and M. M. Potter.

[1]H. R. Child, M. K. Wilkinson, J. W. Cable, W. C. Koehler, and E. O. Wollan, Phys. Rev. 131, 922 (1963).
[2]J. H. Van Vleck, *The Theory of Electric and Magnetic Susceptibilities* (Oxford U. P., Oxford, England, 1932).
[3]G. T. Trammell, Phys. Rev. 131, 932 (1963).
[4]B. R. Cooper, Phys. Rev. 163, 444 (1967).
[5]Y. L. Wang and B. R. Cooper, Phys. Rev. 185, 696 (1969).
[6]D. Pink, J. Phys. C 1, 1246 (1968).
[7]Y. Y. Hsieh and M. Blume, Phys. Rev. B 6, 2684 (1972).
[8]B. R. Cooper, in *Magnetic Properties of Rare Earth Metals*, edited by R. J. Elliott (Plenum, New York, 1972), p. 17.
[9]R. J. Birgeneau, AIP Conf. Proc. 10, 1664 (1973).
[10]T. M. Holden, E. C. Svensson, W. J. L. Buyers, and O. Vogt, *Neutron Inelastic Scattering* (IAEA, Vienna, 1972), p. 553.
[11]See, for instance, W. E. Wallace, F. Kissell, E. Segal, and R. S. Craig, J. Phys. Chem. Solids 30, 13 (1969); E. Bucher, J. P. Maita, and A. S. Cooper, Phys. Rev. B 6, 2709 (1972).
[12]B. R. Cooper and O. Vogt, Phys. Rev. B 1, 1211 (1970); *ibid.* 1, 1218 (1970).
[13]B. D. Rainford, K. C. Turberfield, G. Busch, and O. Vogt, J. Phys. C 1, 679 (1968).
[14]R. J. Birgeneau, E. Bucher, L. Passell, and K. C. Turberfield, Phys. Rev. B 4, 718 (1971).
[15]B. D. Rainford and J. C. Gylden Houmann, Phys. Rev. Lett. 26, 1254 (1971).
[16]R. J. Birgeneau, J. Als-Nielsen, and E. Bucher, Phys. Rev. Lett. 27, 1530 (1971); Phys. Rev. B 6, 2724 (1972).
[17]K. C. Turberfield, L. Passell, R. J. Birgeneau, and E. Bucher, Phys. Rev. Lett. 25, 752 (1970); J. Appl. Phys. 42, 1746 (1971); R. J. Birgeneau, E. Bucher, J. P. Maita, L. Passell, and K. C. Turberfield, Phys. Rev. B 8, 5345 (1973).
[18]H. B. Moller and J. C. Gylden Houmann, Phys. Rev. Lett. 16, 737 (1966).
[19]Our measurements of $T_N$. This value has recently been confirmed by N. H. Andersen, P. E. Gregers-Hansen, E. Holm, and F. B. Rasmussen, in Proceedings of the International Congress on Magnetism, Moscow, 1973 (unpublished).
[20]F. Levy, Phys. Kondens. Mater. 10, 85 (1969).
[21]R. J. Birgeneau, J. Phys. Chem. Solids 33, 59 (1972).
[22]B. Grover, Phys. Rev. 140, A1944 (1965).
[23]B. N. Brockhouse, *Inelastic Scattering of Neutrons in Solids and Liquids* (IAEA, Vienna, 1961), p. 113.
[24]G. Dolling and H. Nieman, Nucl. Instrum. Methods 49, 117 (1967).
[25]M. T. Hutchings, in *Solid State Physics*, edited by F. Seitz and D. Turnbull (Academic, New York, 1964), Vol. 16, p. 227.
[26]W. J. L. Buyers, T. M. Holden, E. C. Svensson, R. A. Cowley, and M. T. Hutchings, J. Phys. C 4, 2139 (1971).
[27]O. Vogt (private communication).
[28]M. F. Collins, V. K. Tondon, and W. J. L. Buyers, Int. J. Magn. 4, 17 (1973).
[29]G. Busch, J. Appl. Phys. 38, 1386 (1967).
[30]T. Kasuya, *Magnetism IIB*, edited by G. T. Rado and H. Suhl (Academic, New York, 1966), p. 215.
[31]J. S. Smart, *Effective Field Theories of Magnetism* (Saunders, Philadelphia, 1966).
[32]T. M. Holden and W. J. L. Buyers, Phys. Rev. B 9, 3797 (1974).
[33]W. J. L. Buyers, T. M. Holden, and A. Perreault (unpublished).
[4]T. M. Holden, B. M. Powell, and A. D. B. Woods, J. Appl. Phys. 39, 457 (1968).